REFERENCES

1) Hinton, E. and Owen, D.R.J., *Finite Element Software for Plates and Shells*, Pineridge Press Ltd., Swansea, UK, 1984

2) Barzegar, F., Layering of RC Membrane and Plate Elements in Nonlinear Analysis, *Journal of Structural Engineering*, ASCE, pp. 2474-2492, 1988

3) Polak, M.A. and Vecchio, F.J., Nonlinear Analysis of Reinforced Concrete Shells, *Journal of Structural Engineering*, ASCE, pp. 3439-3462, 1993

4) Okamura, H. and Maekawa, K., *Nonlinear Analysis and Constitutive Models of Reinforced Concrete*, Gihodo-Shuppan, Tokyo, 1990

5) Task Committee on Finite Element Idealization of the Committee on Electronic Computation of the Structural Division of American Society of Civil Engineering (ed. Meyer, C.), *Finite Element Idealization*, ASCE, 1987

6) Zienkiewicz, O.C. and Taylor, R.L., *The Finite Element Method, vol. 2 - Solid and Fluid Mechanics, Dynamics, and Non-Linearity*, McGraw Hill Book Co., 4th ed., 1991

7) Harmon, T.G. and Ni, Z.Y., Shear Strength of Reinforced Concrete Plates and Shell Determined by Finite Element Analysis using Layered Elements, *Journal of Structural Engineering*, ASCE, pp. 1141-1157, 1989

8) Li, B., Maekawa, K. and Okamura, H., Contact Density Model for Stress Transfer Across Cracks in Concrete, *Journal of the Faculty of Engineering*, University of Tokyo (B), Vol. 40, No. 1, pp. 9-52, 1989

9) Kato, B., Mechanical Properties of Steel under Load Cycles Idealizing Seismic Action, *CEB Bulletin D'Information*, No. 131, pp. 7-27, 1979

10) Steven, N.J., Uzumeri, S.M. and Collins, M.P., Reinforced Concrete Subjected to Reversed Cyclic Shear - Experiments and Constitutive Model, *ACI Structural Journal*, pp. 135-146, 1991

11) Polak, M.A., *Reinforced Concrete Shell Elements Subjected to Bending and Membrane Loads*, Ph.D. Thesis, University of Toronto, Toronto, Canada, 1992

12) Aghayere, A.O. and MacGregor, J.G., Tests of Reinforced Concrete Shells under Combined In-plane and Transverse Loads, *ACI Structural Journal*, pp. 615-622, 1990

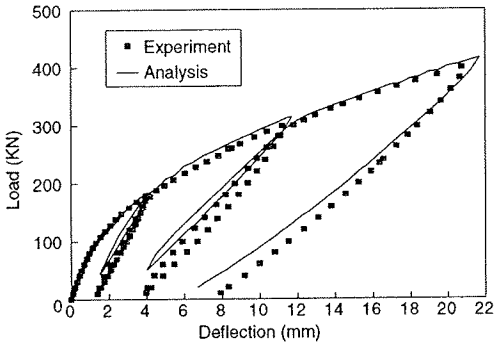

Fig. 24 Load deflection at load point F ($-w_F$) of box culvert

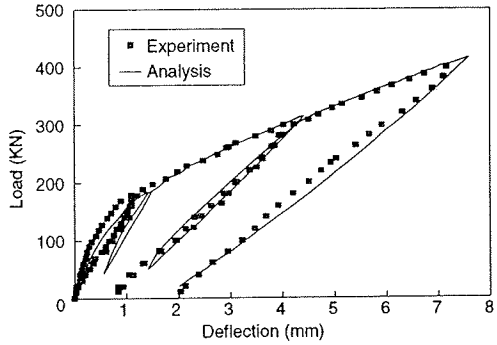

Fig. 25 Load deflection at point A ($-u_A$) of box culvert

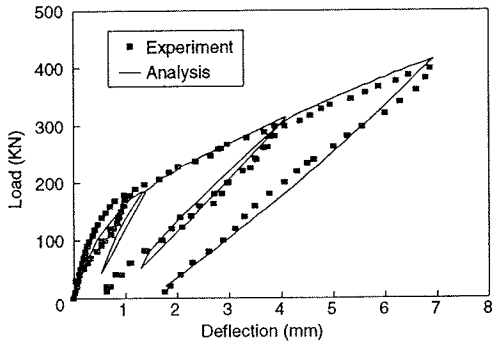

Fig. 26 Load deflection at point B ($-u_B$) of box culvert

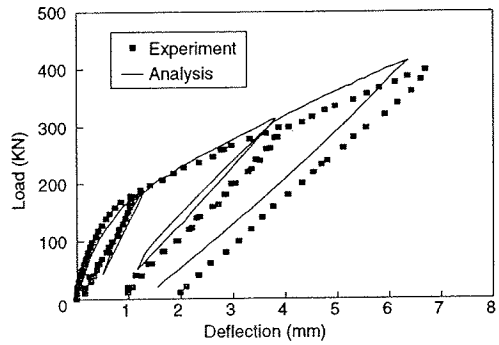

Fig. 27 Load deflection at point C ($-u_C$) of box culvert

9. CONCLUSIONS

A path-dependent nonlinear finite element model has been developed for the analysis of reinforced concrete shells. Through layered formulation, the model has successfully utilized the path-dependent constitutive models of cracked concrete, which consider concrete tension stiffening and compression softening, and reinforcing bar under one dimensional stress condition. Cracked concrete is modeled as an orthotropic nonlinear material using smeared, multi-directional fixed crack approach.

A serendipity eight node isoparametric element was used for modeling plain and reinforced concrete by utilizing layered formulation. A distinctive characteristic of the element is its capability to simulate the behavior of shell elements under cyclic and reversed cyclic loading. A reduced integration scheme was used to avoid shear locking problems. Nonlinear geometrical effects were accounted for by using total Lagrangian formulation. Reissner-Mindlin formulation was applied to take shear deformation into account which is important in the case of thick shells.

In comparison with test data, good predictions were obtained in regard to load capacities. Also good predictions were obtained in regard to load-deformation responses of reinforced concrete shell elements under the combination of bending moments and in-plane loads, the combination of in-plane and transverse loads, and under cyclic and reversed cyclic transverse loads.

The cyclic path-dependent three-dimensional reinforced concrete model is thought to be indispensable for dynamic analysis of full model tanks and shell structures. The authors are applying the program COM3 including the three-dimensional path-dependent reinforced concrete shell model to the verification of structural safety and performance of underground three-dimensional reinforced concrete structures.

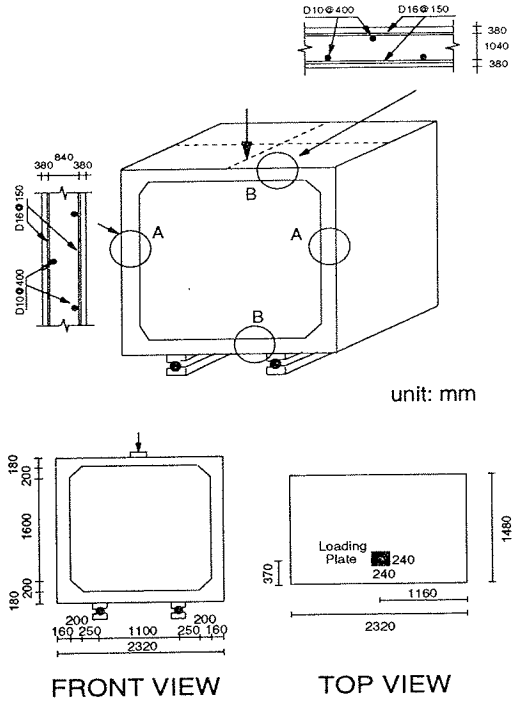

Fig. 22 Detail of box culvert specimen

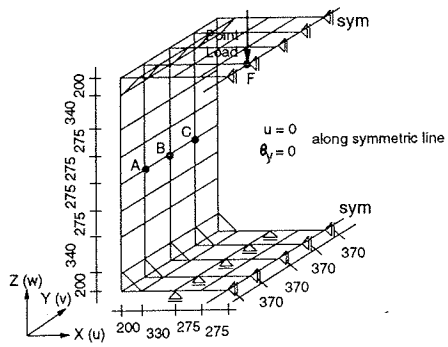

Fig. 23 Element mesh of box culvert

The specimen was loaded from the top slab through a plate, 240 x 240 mm. The location of the loading plate can be seen in **Fig. 22**. Cyclic loads were applied through this loading plate. With this kind of loading, the top slab would be under biaxial bending moments and torsion, the bottom slab was under bending moment and the walls were under a combination of in-plane load, bending moment and torsion.

Due to the symmetry along the direction of width, only half of the box culvert needed to be discretized in the finite element analysis. For top and bottom slabs, 4 x 4 shell elements were used, while 8 x 4 shell elements were adopted for the walls. In each shell element, seven layers were utilized for integration through the depth. Solid elements were used to model the haunches at the corners of the box culvert. Four solid elements were utilized for the haunches in each corner. **Fig. 23** shows the discretization of the box culvert.

Comparisons of the experiment and analysis results are presented in **Figs. 24** through **27** in terms of applied load and deflection at load point and points A, B, and C (See **Fig. 23**), respectively. Generally the analysis shows good prediction for the load-deflection relationship at load point and point A. For points B and C, the analytical predictions of displacement are smaller than data from the experiment.

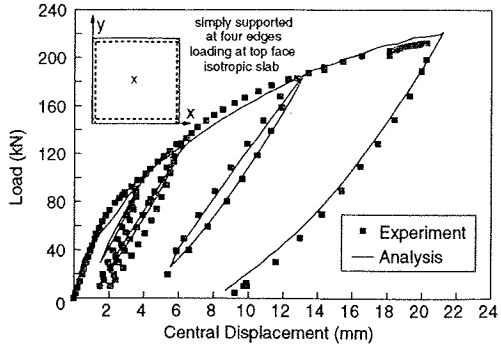

Fig. 18 Response of specimen IS1 (top face loading)

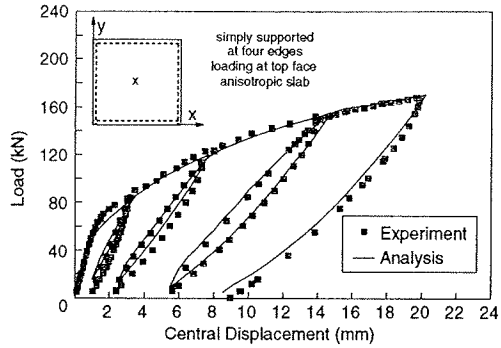

Fig. 19 Response of specimen IS2 (top face loading)

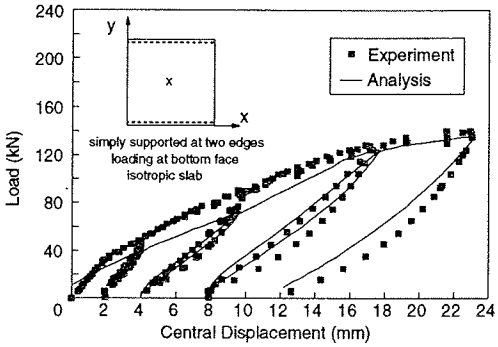

Fig. 20 Response of specimen IS1 (bottom face loading)

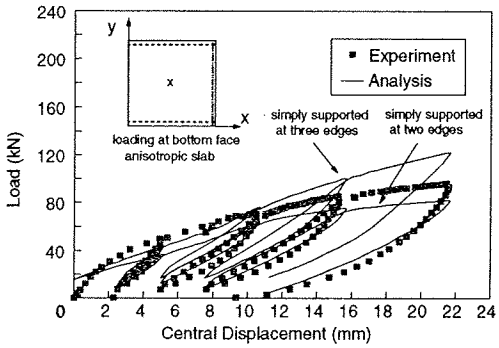

Fig. 21 Response of specimen IS2 (bottom face loading)

For anisotropic slab (IS2), at a smaller deflection an observation similar to the isotropic slab was noticed. At a larger deflection the prediction is higher than the experimental results. In this condition, because of the deflection of slab in the *y*-direction, the slab did not completely contact the *y*-direction support as observed in the experiment. Since the analysis assumed perfect contact between slab and all supports, including the *y*-direction support, higher analytical prediction was observed. In **Fig. 21**, analytical results of anisotropic slab (IS2) under bottom face loading and simply supported at two edges in the *x*-direction are shown. While the prediction under three supports serves as an upper bound prediction, it serves as a lower bound prediction of the experimental results. The actual load-deflection curve should lie between these curves as shown in **Fig. 21**.

8. BOX CULVERT SPECIMEN

The outer dimensions of the box culvert used in the experiment is 2320 mm in length, 2360 mm in height and 1480 mm in depth, with inner dimensions of 2000 x 2000 x 1480 mm. At the corners there were four haunches of 200 x 200 mm in size. The thickness of the wall is 160 mm with two layers of reinforcing bars of 16 mm in diameter with spacing of 150 mm at each side in the height direction with a volumetric ratio of reinforcement is 1.87 %, and two layers of reinforcing bars of 10 mm in diameter with spacing of 400 mm at each side in the depth direction with a volumetric ratio of reinforcement of 0.27 %. The thickness of top and bottom slabs are equal with the same mesh of reinforcement as the wall and a volumetric reinforcement ratio of 1.66 % in the width direction and 0.24 % in the depth direction. Compressive strength of concrete at the time of testing was 50 MPa and the yield stress of reinforcing bars was 400 MPa. Details of specimen are illustrated in **Fig. 22**. The box culvert was simply supported along the depth at a distance from the center of the support to the outer edge of 630 mm. The material and size of the supports were similar to those of the slab test in the previous section.

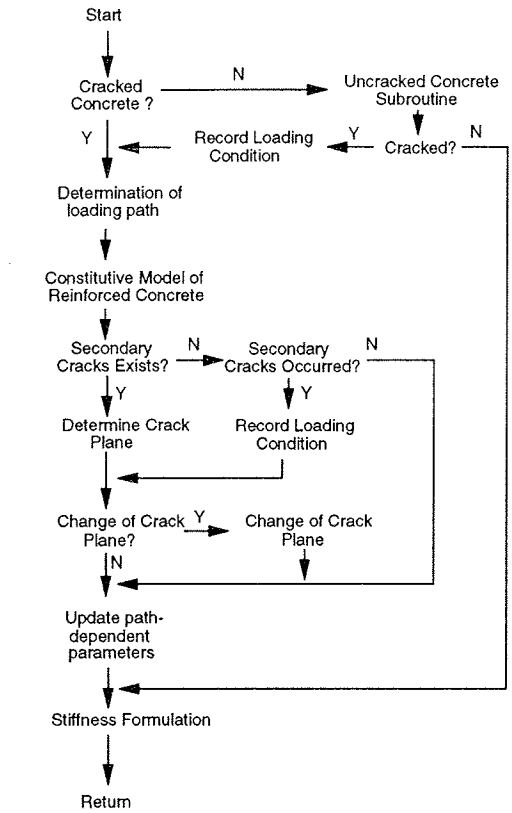

Fig. 16 Flowchart diagram to include two-way active cracks control

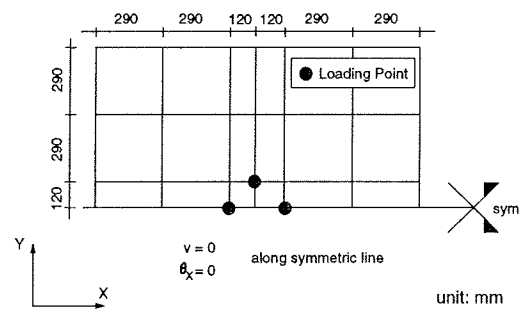

Fig. 17 Element mesh for IS specimens

width is relatively large, was also well predicted. However, in the case where cracking has just occurred, due to complex stress conditions at the closing and opening of cracks, there are some discrepancies in the prediction of cyclic loop in the lower level of displacement.

Finally, comparisons of analyses and experiments for bottom face loading of both isotropic and anisotropic slabs under cyclic loads are given in **Figs. 20** and **21**, respectively.

For isotropic slab (IS1), initial stiffness of the slab from experimental data was observed as being quite high and as decreasing with the occurrence of cracks. This was not observed in the analytical results. Initial stiffness of the analytical result was almost similar to the stiffness of experimental data after cracking. This might happen due to the closing of some cracks when the slab was turned upside down in the experiment. When the deflection is larger, the analytical prediction is almost similar to the experiment.

Table 4 Slab-series test specimens

Specimen	Concrete	Reinforcement						
		x-direction			y-direction			
	f_c' (MPa)	ρ_x (%) [a]	x_1 (mm)	x_2 (mm)	ρ_y (%) [a]	y_1 (mm)	y_2 (mm)	f_y (MPa)
IS-1	37.0	0.78	25	75	0.78	15	85	380
IS-2	37.0	0.78	25	75	0.39	15	85	380

[a] Per layer

x_1 : distance between the center of first re-bar layer in x-direction to the bottom surface of specimen

x_2 : distance between the center of second re-bar layer in x-direction to the bottom surface of specimen

y_1 : distance between the center of first re-bar layer in y-direction to the bottom surface of specimen

y_2 : distance between the center of second re-bar layer in y-direction to the bottom surface of specimen

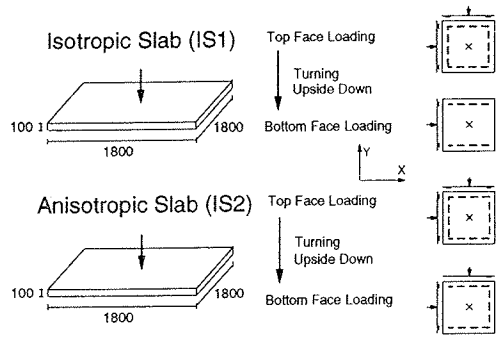

Fig. 15 Experimental work on IS specimens

around the center of the specimen. It should be noted that these two sets of cracks occurred under the same loading condition. In other words, these two sets of cracks were opening (active) at the same loading condition and closing simultaneously in the reversed loading condition.

This condition is different from the case of the reinforced concrete panel, where at one loading condition, only one set of cracks occurs and is active. When the loading is reversed, another set of cracks occurs and becomes active, while the previous set of cracks becomes inactive (closing).

The finite element program was developed to include the possibility for the case of two sets of active cracks working simultaneously. Strain perpendicular to the cracks at each crack point should be checked and updated if it exceeds the previous maximum value in every load step. **Fig. 16** shows the flowchart diagram considering two-way active crack control.

In this analysis, specimens were modeled using a mesh of 6 x 3 elements as shown in **Fig. 17** by facilitating the symmetry of the slab in the y-direction for all cases of loading (See **Fig. 15**). Concrete outside the supports was eliminated in finite element domain since its presence has negligible effect on the computed results. Ten layers per element were used for the integration through the depth. Restart facility in the program was used to change the support condition between the top face and bottom face loading (after the slab was turned upside down).

Tensile strength of concrete is difficult to determine accurately, since it depends on curing conditions, and shrinkage during drying, as well as the size of the specimen. For this analysis, the tensile strength of concrete was adjusted from the experiment data to approximately 50 % of the strength of specimens used for quality control in the laboratory.

Comparisons of analyses and experiments for top face loading of both isotropic and anisotropic slabs under cyclic loads are given in **Figs. 18** and **19**, respectively. The analysis shows good prediction of the envelope curve of load-deflection for both isotropic and anisotropic arrangements of reinforcing bars. The cyclic loop in the case where reinforcing bars in the middle of slabs have been yielding, which also means the crack

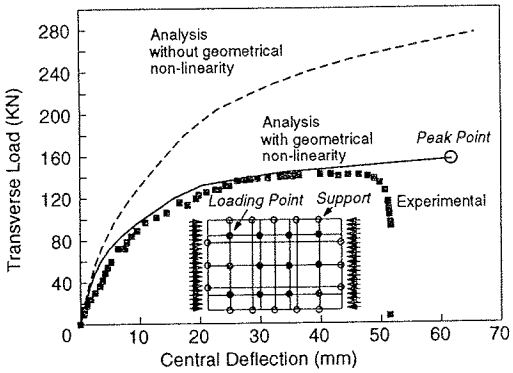

Fig. 13 Response of specimen B1

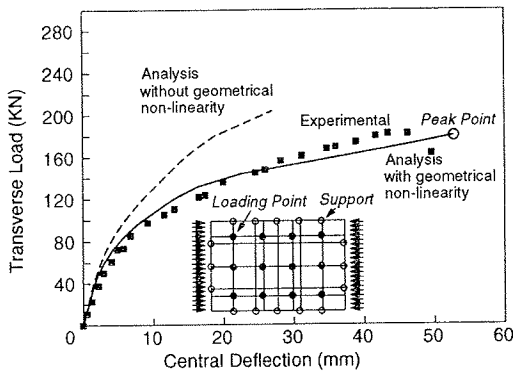

Fig. 14 Response of specimen B2

inclusion of geometrical nonlinearity) and experiments for specimens A1, A2, A3, B1 and B2 are given from **Figs. 10** through **14**.

In general, the model can predict the load-deflection curve of slabs up to failure well. It should be noted that since the analyses were carried out by using an increasing load control, the falling branch of the load-deflection curve could not be obtained. In the case of slab A3, the prediction of cracking load is higher than the experiment although the initial computed stiffness under elastic condition coincides with actual results. This may be attributed to the initial induced tension, due to drying shrinkage, which is not taken into account in the analysis. Further investigation is needed for more accurate prediction of cracking loads.

7. ELEMENTS SUBJECTED TO CYCLIC AND REVERSED CYCLIC TRANSVERSE LOADS

Experimental data for monotonic loading under different kinds of loading are available, however, there is insufficient data available on the behavior of reinforced concrete shells under cyclic loading. Therefore, a series of tests consisting of two slabs was conducted under cyclic and reverse cyclic transverse point loads at the center of the slabs.

Two slabs with different arrangements of reinforcing bars (isotropic and anisotropic) were prepared to check finite element formulation's capability of predicting behavior under cyclic loading. The slab specimen's size was 1800 x 1800 mm. In the isotropic slab (IS1), reinforcement ratios in x- and y-directions were equal, while in the anisotropic slab (IS2), the reinforcement ratio in the x-direction was twice that of the y-direction. Reinforcement, in both specimens, was placed in two layers (top and bottom) in each of the two orthogonal directions. In the same direction, reinforcement ratios for the top and bottom layers was equal. Diameter of the reinforcing bars used in the specimens was 10 mm. To obtain different reinforcement ratios, the spacing between reinforcing bars was adjusted. The material properties of specimens are given in **Table 4**.

Both slabs were simply supported around the perimeter of the center of the slabs at 1400 x 1400 mm. Hence, only this part was analyzed. The supports consisted of two plates of 25 mm thickness and 100 mm width and a steel rod of 40 mm in diameter which was placed between the two bearing plates to avoid local damage around the supports. The purpose of casting the specimens in larger sizes of 1800 x 1800 mm was to obtain enough anchorage zone for reinforcing bars. Transverse cyclic load was applied at the center of the slab through loading plate with a diameter of 240 mm. Three cycles of loading were applied.

To obtain data under reversed cyclic loading, the slab was turned upside-down. Support for the slab with isotropic arrangement of reinforcement (IS1) was changed simply supported at two sides along the x-direction, while the slab with anisotropic arrangement of reinforcement was supported at three edges, both shown in **Fig. 15**. Then three cycles of loading were also applied to the slab's center on this side.

Concrete cracks at the center were observed in two directions. One direction radiated from the center of the specimen, where the load was applied, to the four corners of the slab. The other direction was radial cracks

Table 3 University of Alberta slab specimens[12)]

Specimen	Concrete Properties		Reinforcement			In-plane Load
	f_c' (MPa)	E_c (MPa)	ρ_x (%) [a]	ρ_y (%) [a]	f_y (MPa)	(KN/m)
A1	32.3	22,970	0.336	0.390	504	962
A2	32.3	23,010	0.350	0.400	504	765
A3	32.3	23,150	0.344	0.400	504	0
B1	40.3	25,580	0.500	0.590	504	874
B2	40.2	25,550	0.500	0.590	504	634

E_c : modulus of elasticity of concrete

[a] Per layer

Note: x-direction is normal to the applied in-plane load

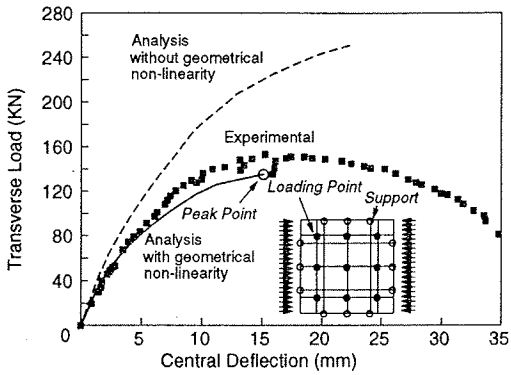

Fig. 10 Response of specimen A1

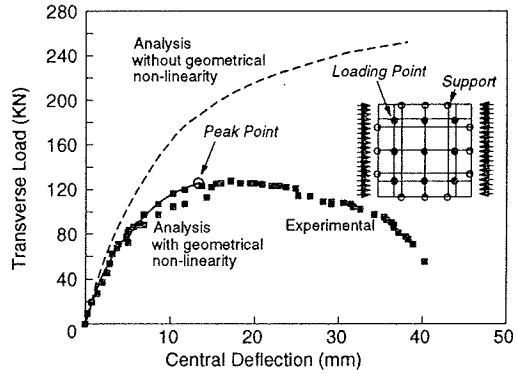

Fig. 11 Response of specimen A2

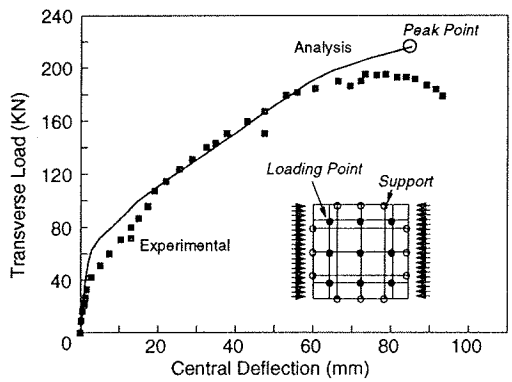

Fig. 12 Response of specimen A3

As mentioned earlier, since the stress distribution across the slabs is not uniform, more elements are needed to model the slabs using finite elements. A-type slabs were divided into a mesh of 6 x 6 elements, while the B-type slabs were divided into a mesh of 6 x 8 elements, as shown in **Figs. 10** through **14**. Along the thickness, seven layers per element were used for the integration through the depth. Since the slab's thickness is very small compared to its width and furthermore due to the presence of relatively high in-plane loads, geometrical nonlinearity was significant for these cases. This series of tests provide additional verification for the capabilities of the analytical procedure. Comparisons of analyses (with and without the

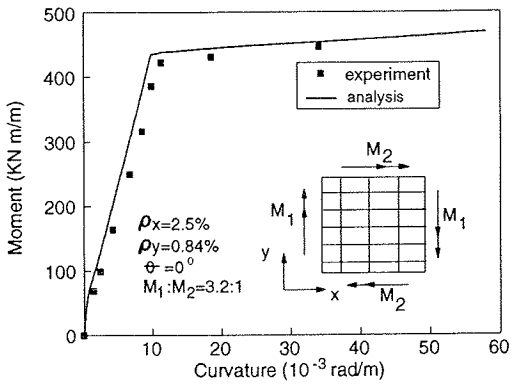

Fig. 8a SM3 under biaxial bending moments. (stronger reinforcement)

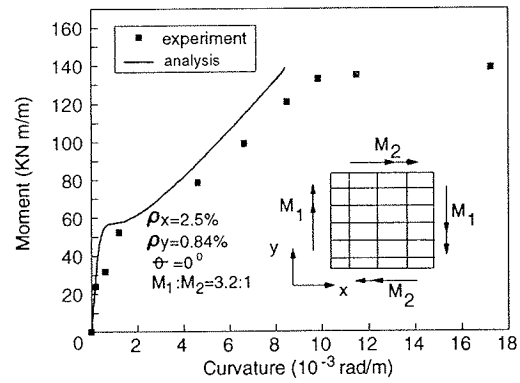

Fig. 8b SM3 under biaxial bending moments (weaker reinforcement)

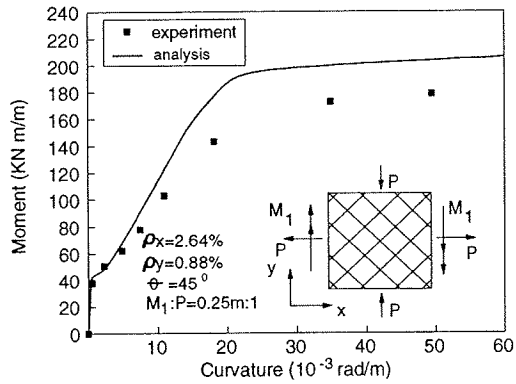

Fig. 9 SM4 under bending moment and in-plane loads (skew reinforcement)

6. ELEMENTS SUBJECTED TO IN-PLANE AND TRANSVERSE LOADS

A series of tests from the University of Alberta[12] was used for the verification of the behavior of shell elements subjected to combined loads of in-plane and transverse loads. Compared to the previous tests, loading condition is not uniform around the element. Depending on the slab's aspect ratio, the test slabs were divided into various groups. Type-A slabs were square with outside dimensions of 1,830 x 1,830 mm, while type-B slabs were rectangular with the dimensions of 2,744 x 1,830 mm.

The slab's thickness was approximately 65 mm. The specimens were reinforced with two layers of deformed bars placed in orthogonal directions, with the reinforcement ratios for the top and bottom layers being equal. The specimens were simply supported at certain points around the perimeter. In-plane loads were applied along the outside layers of reinforcement while transverse loads were applied at nine points for the A-type slabs, and at 12 points for the B-type slabs [See **Figs. 10** and **13**]. A sequential loading pattern was applied to the slab, in-plane load was applied first to the full magnitude, and kept constant. Then, out-of-plane load was applied gradually until the failure of the specimen. Specimens A1 and A2 were subjected to both out-of-plane and in-plane loads, with different intensities of in-plane load. Specimens A3 was only subjected to out-of plane load. Like specimens A1 and A2, specimens B1 and B2 were also subjected not only to out-of-plane loads, but also in-plane loads of different intensities. The details of specimens and the amount of in-plane loads are given in **Table 3**.

Table 2 University of Toronto slab specimens[11]

Specimen	Concrete	Reinforcement					Applied [b] Loading
	f_c' (MPa)	θ (degrees)	ρ_x (%) [a]	f_{yx} (MPa)	ρ_y (%) [a]	f_{yy} (MPa)	M_1:M_2:P
SM1	47	0	1.25	425	0.42	430	1:0:0
SM2	62	0	1.25	425	0.42	430	0.25 m:0:1
SM3	56	0	1.25	425	0.42	430	3.2:1:0
SM4	64	45	1.32	425	0.44	430	0.25 m:0:1

[a] Per layer [b] See **Figs. 6** to **9**

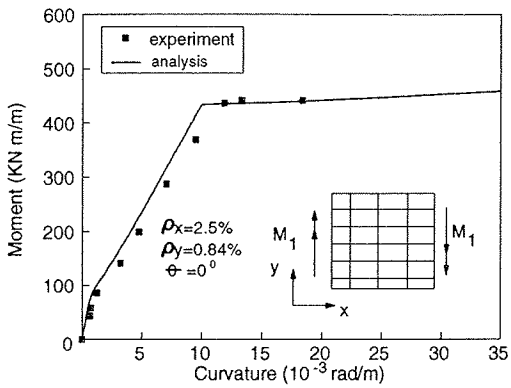

Fig. 6 SM1 under bending moment

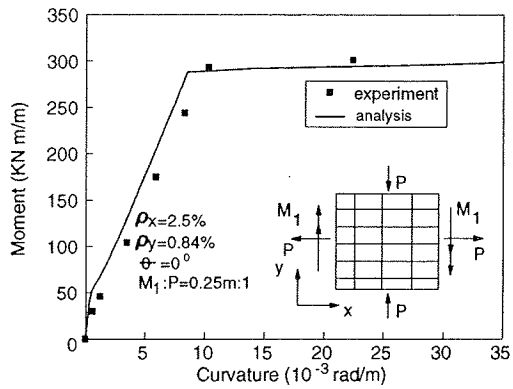

Fig. 7 SM2 under bending moment and in-plane loads

loading conditions were different. SM1 was loaded in pure bending moment to the stronger reinforcement. SM2 was loaded in bending moment (as in SM1) and biaxial plane stress with tension applied to the stronger reinforcement and compression applied to the weaker reinforcement. SM3 was loaded in biaxial bending, while SM4 was loaded in the same manner as SM2, only the direction of reinforcement was oriented at a 45° angle with respect to the applied loads. How skew reinforcement influences the tensile response is the main interest in specimen SM4. The details of specimens and loading conditions are given in **Table 2**.

In specimens SM1, SM2 and SM3, due to the reinforcing bars and loading configurations, stress distribution across the shell will be constant. Therefore, only one element was used to model the specimen. For specimen SM4, due to skew reinforcement, torsion will occur inside the specimen and stress distribution across the specimen will not be uniform, so a mesh of 16 equal-size elements was used to model the specimen. Ten layers per element were used for the integration through the depth of the specimen.

Comparisons of analyses and experiments for the four cases are given in **Figs. 6** to **9**. Generally the results from the analysis predicted the behavior of specimens well in terms of yield and ultimate moments, except for specimen SM4 where the prediction of ultimate moment is higher than the experiment results. The discrepancy may occur due to the reorientation of cracks and the formation of secondary cracks when the weak reinforcement yielded as reported from the experimental works.[11] A fixed crack approach used in this analysis implies that it does not take into account the possibility of the slight reorientation of the cracks propagation direction. The direction of propagation of cracks is assumed to follow the direction of initially induced cracks. This assumption may cause the model to supply additional stiffness to the element to resist the load which causes higher prediction of ultimate moment. Fixed crack approach was adopted in representing cracks in the analysis, since it is indispensable in the path-dependent modeling of cracks under cyclic stresses. The development of fixed crack approach which takes into account the slight change of crack propagation during loading will be the next stage of this research.

Table 1 Material properties of SE-specimens[10)]

Specimen	Concrete	Reinforcement				
	f_c' (MPa)	θ (degrees)	ρ_x (%) [a]	f_{yx} (MPa)	ρ_y (%) [a]	f_{yy} (MPa)
SE8	37.0	0	1.465	492	0.49	479
SE9	44.2	0	1.465	422	1.465	422

f_c' : compressive strength of concrete
θ : angle of the orientation of reinforcing bars to x-direction of specimen
ρ_x , ρ_y : reinforcement ratio in x- and y- directions
f_{yx} , f_{yy} : yield strength of steel in x- and y- directions : [a] Per layer

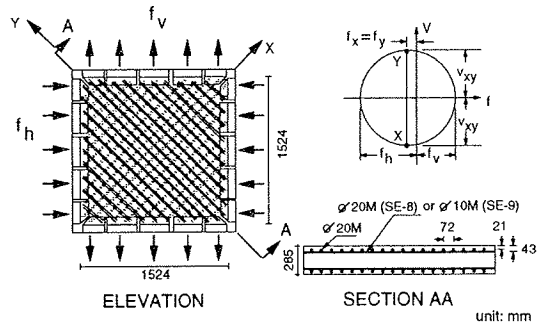

Fig. 3 Reinforcement layout and application of stresses of SE-8 and SE-9

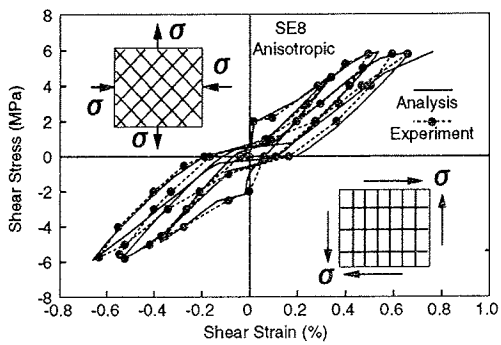

Fig. 4 Response of specimen SE-8

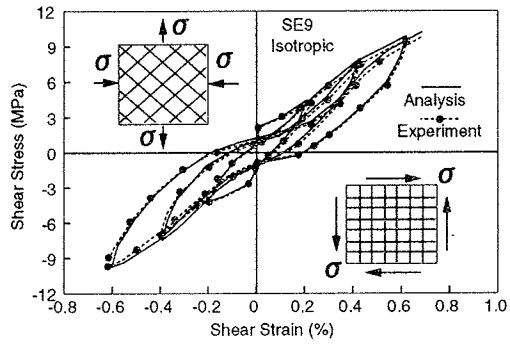

Fig. 5 Response of specimen SE-9

The comparisons between analytical and experimental results are shown in **Figs. 4** and **5**. The analytical results show good agreement with what was observed in the experiments not only in loading, but also in unloading and reloading conditions. From these comparisons, the capability of the program to predict the behavior of shell elements under in-plane reversed cyclic shear load was confirmed.

5. ELEMENTS SUBJECTED TO BENDING AND IN-PLANE LOADS

A series of tests from the University of Toronto[11)] was used for the verification of the behavior of shell elements subjected to the combination of bending moment and in-plane loads. The size of the specimens was 1524 x 1524 with two layers of deformed bars in each of the two orthogonal directions. To verify the model of tension stiffening, the reinforcement was made much higher in one direction than the other. The specimen thickness was 316 mm. The specimens were subjected to various loading conditions of bending moment and in-plane loads. Specimens SM1, SM2, and SM3 were reinforced in the same manner, only the

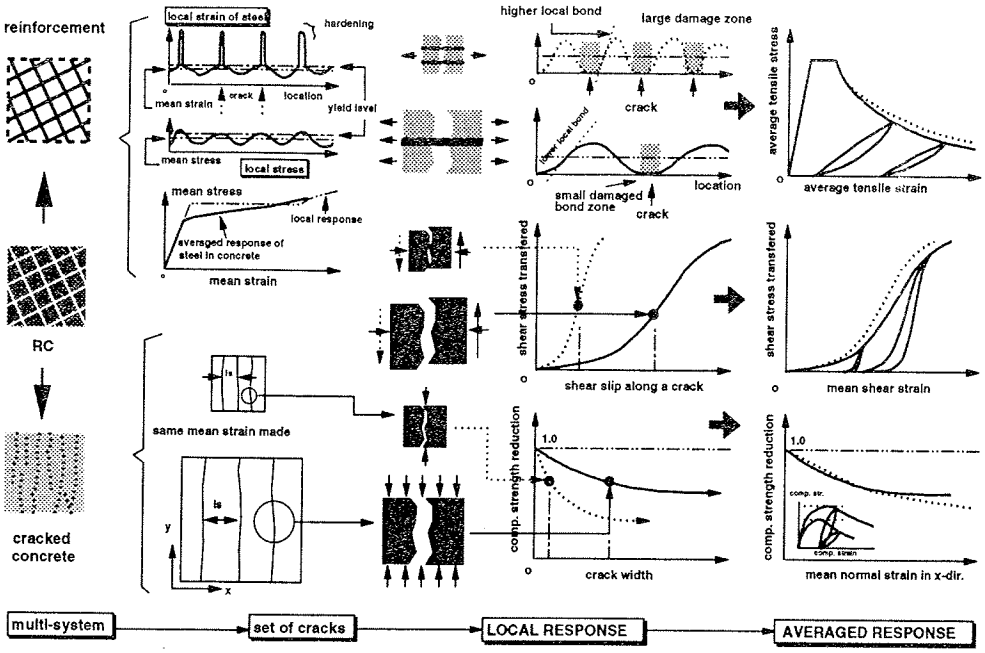

Fig. 2 Composition of in-plane constitutive laws of reinforced concrete

reversed cyclic loading and the assumption of steel stress distribution patterns are used for calculating the mechanical behaviors of reinforcing bars in concrete under reversed cyclic loadings.[4)]

The schematic diagram of constitutive models used in this study is shown in **Fig. 2** and detailed discussion of the constitutive models can be found in reference 4).

In this analysis, the open-closure control of two-way cracks was enhanced in accordance with the cracking conditions of reinforced concrete slabs subjected to out-of-plane loads. These details are stated in chapter 7.

4. ELEMENTS SUBJECTED TO IN-PLANE REVERSED CYCLIC SHEAR

First of all, the capability of finite element analysis was tested to predict the behavior of concrete panels subjected to in-plane reversed cyclic shear. The specimens were full size shell elements reinforced with deformed reinforcing bars.

The experimental works investigated in this section were done by Stevens et. al.[10)] Full size shell elements were tested using the Shell Element Tester at the University of Toronto. The specimens were loaded in in-plane reversed cyclic shear loading. One of the specimens had isotropic arrangement of reinforcement (SE-9) and the other had anisotropic arrangement (SE-8).

The size of the specimen was 1524 x 1524 mm with two layers of deformed bars in each of the two orthogonal directions. The thickness of the specimen was 285 mm. Details of material properties can be found in **Table 1**. The reinforcement layout and the application of stresses can be found in **Fig. 3**. Reversed cyclic shear loads were applied along the directions of reinforcement, by applying equal tension and compression forces (f_v=f_h in **Fig. 3**) in the two orthogonal directions at 45° to the reinforcement.

Since the force distribution is uniform across the element, only one finite element was used to predict the response of the specimen. The number of layers used per element was two (the minimal number of layers installed in the program), although one layer is sufficient for in-plane pure shear loading where stress distribution along the thickness is uniform.

One more relationship between rotation normal to the mid-surface of the shell and drilling forces is needed to anticipate the assembly of shell elements in the same plane. This relationship is written as,

$$\{M_z\}=[K_{99}]\{\varsigma_z\} \tag{10}$$

where rotation normal to the mid-surface of the shell is obtained from:

$$\varsigma_z=\frac{1}{2}\left(\frac{\partial v}{\partial x}-\frac{\partial u}{\partial y}\right)-\theta_z \tag{11}$$

Finally, Eq. (7), Eq. (9), and Eq. (10) can be combined and the relationship between generalized forces and generalized strains is developed.

Geometrical nonlinearity which is significant in the case of thin shell members is accounted for by total Lagrangian formulation. It makes use of Green-Lagrange strain tensors and the second Piola-Kirchoff stress tensor.[6]

3. MATERIAL MODELING

A multi-directional smeared fixed crack approach[4] was incorporated in the material modeling of cracked concrete. It consists of a tension stiffening model, a compression model and a shear transfer model. A model of reinforced concrete has been constructed by combining those three models with a model of reinforcing bars in concrete. Prior to cracking, concrete is modeled as an elasto-plastic and fracture material with the introduction of fracture parameter as an indicator of the reduction of elastic modulus in the unloading process.[4]

Modeling of concrete under tensile stress is independent of the crack's spacing, the direction of reinforcing bars and the reinforcement ratio. It is modeled in the form of average stress versus average strain of concrete. After average strain reaches cracking strain, concrete stress decreases gradually taking into account the tension stiffening effect. In the reversed cyclic loadings, concrete stress is the sum of stress transmitted from the reinforcing bars plus that transmitted from the closing of the cracks.[4]

The modeling of concrete under compressive stress is formed based on an elasto-plastic fracture model similar to the pre-cracking model. The effect of compression softening due to the presence of transverse cracks, which causes the reduction of strength and stiffness, is accounted for by modifying the value of fracture parameter for the cracked concrete from the uncracked one as a function of the strain perpendicular to the crack plane.[4] The degradation of stiffness is believed due to the reduction of the capability of concrete to resist compressive stress in the vicinity of cracks on account of the roughness of crack surfaces. Therefore, in case of very large cracks this effect will not continue increasing and the reduction factor has the minimum limit.

The modeling of concrete under shear stress is based on the contact density function.[8] The model defines the geometrical form of a crack based on two parameters, shear displacement and crack width, and is applicable to any loading histories. The model expresses shear stress in terms of the ratio of those two parameters. Compressive stress associated with shear displacement is formulated in the same manner. In reversed cyclic loading, shear stiffness of the uncracked portion, which causes a sudden increase in the closing of the crack, is included.[4]

The modeling of reinforcing bars in concrete is given in the form of average stress versus average strain in use of bilinear line. It has a clear offset point for initiation of strain hardening with the strain hardening rates held constant and is derived for the post-yielding model of bar under monotonic loading. The strain hardening rate is influenced by steel ratio, angle between the bars and the normal to the crack plane, yield strength of the bar, compressive strength of concrete and the bond.[4] Kato's model[9] for bare bars under

$$\begin{Bmatrix} \sigma_x^i \\ \sigma_y^i \\ \sigma_{xy}^i \end{Bmatrix} = \begin{bmatrix} D_{11} & D_{12} & D_{13} \\ D_{21} & D_{22} & D_{23} \\ D_{31} & D_{32} & D_{33} \end{bmatrix} \left\{ \begin{Bmatrix} \bar{\varepsilon}_x \\ \bar{\varepsilon}_y \\ \bar{\gamma}_{xy} \end{Bmatrix} + z \begin{Bmatrix} \phi_x \\ \phi_y \\ \phi_{xy} \end{Bmatrix} \right\} \tag{6}$$

Integration through the thickness of element is taken through layered-element formulation. In the depth of its mid-surface, one integration point was used for each layer of panel. Each layer is classified as plain concrete or reinforced concrete layer where reinforcing bars are smeared in the layer (See **Fig. 1**). This classification is important to define the actual location of reinforcing bars for the calculation of internal bending moment of the shells. If the shell element is thin enough to assume the full concrete volume for confining free elongation of bars by bond action, it is assumed that the concrete as a whole contributes uniformly to the tension stiffening model.

However, if the large thickness of shells brings about localized cracking inside it, some layer could be distinguished from the reinforced concrete volume. This study covers reinforced concrete thin shells in which tension stiffening used in every layer – with and without reinforcement – is constant and based on tension stiffening[4] with reinforcement smeared throughout the concrete. Average stress vs. average strain relationship of steel reinforcement in concrete is also derived based on this assumption.[4]

Constitutive equations are applied through the integration point and as a result in-plane stresses of concrete and reinforcement are obtained separately based on the smeared reinforcement along the thickness of the element. Internal forces are calculated by integrating the corresponding stresses from each layer over the thickness of the element. In the process of integration the stress of reinforcement is calculated based on the actual location of steel reinforcement. The advantages of layered element compared to three-dimensional solid element models are the large reduction in structural degrees of freedom required for the analysis and the relative ease in interpreting the computer output.[7] Moreover, constitutive models for reinforced concrete panels are simpler and better developed compared to the three-dimensional reinforced concrete solid element.

By integrating in-plane stresses in every layer, membrane forces N_i and bending moments M_i can be obtained as,

$$\begin{aligned} N_x &= \int_{-t/2}^{t/2} \sigma_x \, dz = \sum_1^n \sigma_x^i \, t^i & M_x &= \int_{-t/2}^{t/2} z\sigma_x \, dz = \sum_1^n z \, \sigma_x^i \, t^i \\ N_y &= \int_{-t/2}^{t/2} \sigma_y \, dz = \sum_1^n \sigma_y^i \, t^i & M_y &= \int_{-t/2}^{t/2} z\sigma_y \, dz = \sum_1^n z \, \sigma_y^i \, t^i \\ N_{xy} &= \int_{-t/2}^{t/2} \tau_{xy} \, dz = \sum_1^n \sigma_{xy}^i \, t^i & M_{xy} &= \int_{-t/2}^{t/2} z\tau_{xy} \, dz = \sum_1^n z \, \sigma_{xy}^i \, t^i \end{aligned} \tag{7}$$

where n is number of layers through the thickness and t^i is the thickness of layer i.

Transverse shear strains including shear deformations are in the form of:

$$\begin{aligned} \gamma_{xz} &= \frac{\partial w}{\partial x} + \theta_y \\ \gamma_{yz} &= \frac{\partial w}{\partial y} - \theta_x \end{aligned} \tag{8}$$

Shear force is obtained as,

$$\begin{Bmatrix} V_x \\ V_y \end{Bmatrix} = \begin{bmatrix} G_c & 0 \\ 0 & G_c \end{bmatrix} \begin{Bmatrix} \gamma_{xz} \\ \gamma_{yz} \end{Bmatrix} \tag{9}$$

where G_c is out-of-plane shear modulus of concrete. Since the transverse shear deformation before and after cracking is generally smaller compared with the flexural one, the elastic shear modulus of concrete was used in this study.

As mentioned earlier, there are six degrees of freedom in every nodal point of the element. These degrees of freedom are defined as,

$$\{d\} = \begin{bmatrix} u & v & w & \theta_x & \theta_y & \theta_z \end{bmatrix}^T \tag{1}$$

where u, v, w are displacements in x-, y-, z-direction, and θ_x, θ_y, θ_z are rotations along x-, y-, z-axis. The degrees of freedom are located in the mid-surface of the element thickness.

A typical Reissner-Mindlin shell with membrane and bending element terms is shown in **Fig. 1** and if the xy-plane is taken as the reference plane then the shell displacements can be expressed as:

$$\begin{aligned} u(x,y,z) &= u(x,y) + z\theta_y(x,y) \\ v(x,y,z) &= v(x,y) - z\theta_x(x,y) \\ w(x,y,z) &= w(x,y) \end{aligned} \tag{2}$$

where $u(x,y)$, $v(x,y)$, $w(x,y)$, $\theta_x(x,y)$, and $\theta_y(x,y)$ are in-plane and transverse deflections and rotations of the normal in the yz- and xz-planes, respectively.

Fig. 1 gives an illustration of layered element and forces acting on the shells.

In the layered element formulation, the shell is divided into several layers of panel where the two-dimensional constitutive models were applied to take into account material nonlinearities. In-plane strains in each layer can be written as,

$$\begin{aligned} \varepsilon_x^i &= \bar{\varepsilon}_x + z\,\phi_x \\ \varepsilon_y^i &= \bar{\varepsilon}_y + z\,\phi_y \\ \gamma_{xy}^i &= \bar{\gamma}_{xy} + z\,\phi_{xy} \end{aligned} \tag{3}$$

where $\varepsilon_x^i, \varepsilon_y^i$, and γ_{xy}^i are in-plane strains in the xy plane in layer i; $\bar{\varepsilon}_x, \bar{\varepsilon}_y$, and $\bar{\gamma}_{xy}$ are in-plane strains in the xy plane in the mid-surface of element thickness, while ϕ_x, ϕ_y and ϕ_{xy} are bending and twisting curvatures. z is the distance from the mid-surface of element thickness to the mid-surface of layer i. The generalized strains in the mid-surface of element thickness and the curvatures are defined as:

$$\begin{aligned} \bar{\varepsilon}_x &= \frac{\partial u}{\partial x} & \phi_x &= \frac{\partial \theta_y}{\partial x} \\ \bar{\varepsilon}_y &= \frac{\partial v}{\partial y} & \phi_y &= -\frac{\partial \theta_x}{\partial y} \\ \bar{\gamma}_{xy} &= \frac{\partial u}{\partial y} + \frac{\partial v}{\partial x} & \phi_{xy} &= \frac{\partial \theta_y}{\partial y} - \frac{\partial \theta_x}{\partial x} \end{aligned} \tag{4}$$

In-plane stresses in every layer can be obtained from in-plane strains in each layer through the application of two-dimensional constitutive models of reinforced concrete and can be generally written as,

$$\begin{Bmatrix} \sigma_x^i \\ \sigma_y^i \\ \sigma_{xy}^i \end{Bmatrix} = \begin{bmatrix} D_{11} & D_{12} & D_{13} \\ D_{21} & D_{22} & D_{23} \\ D_{31} & D_{32} & D_{33} \end{bmatrix} \begin{Bmatrix} \varepsilon_x^i \\ \varepsilon_y^i \\ \gamma_{xy}^i \end{Bmatrix} \tag{5}$$

By substituting Eq. (3) into the strains of the right hand side of Eq. (5), Eq.(6) can be written as,

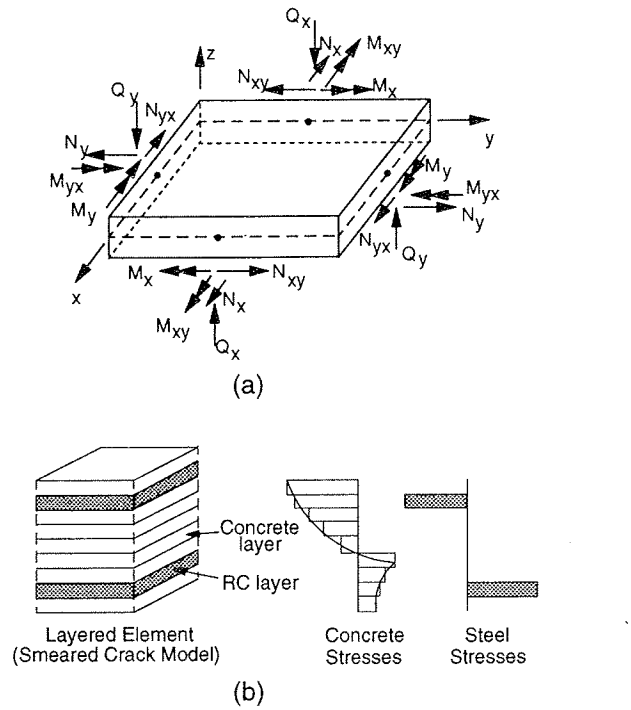

Fig. 1 Shell element (a) Forces acting on RC shells; (b) Layered element

The element needs to be based on three-dimensional elasticity formulation and be capable of modeling both thin and thick shells without experiencing shear locking. It is also important for the element to be able to include shear deformation in the formulation essential in thick shell problems.

Based on the given requirements, an eight-node serendipity isoparametric element with six degrees-of-freedom in each node, three translations and three rotations, was used in the analysis. The last degree of freedom is rotation about the normal to the plane of the element and sometimes referred as the drilling degree of freedom.[6] Fictitious stiffness is given in this degree of freedom to avoid ill-conditioning, which may occur if all elements meeting at a node are co-planar.

The Reissner-Mindlin formulation was adopted to make consideration of shear deformation of concrete shells possible. The formulation is made based on the following assumptions:

1. Normals to the mid-surface remain straight but not necessarily normal to the mid-surface after deformation.

2. Stresses normal to the mid-surface are negligible.

The first assumption implies that shear deformation is included in the formulation while the second assumption indicates that the resultant of out-of-plane stress (z-direction) is zero. The second assumption does not preclude the development of normal stresses in the concrete in the z-direction, provided out-of-plane reinforcement is present to counterbalance these stresses.

As the thickness of shell is decreasing and approaching the limiting thickness, shear locking will likely occur when exact order of numerical integration is used.[6] This locking happens when shear strain energy terms in the potential energy impose the constraints of shear deformations, $\gamma_{xz}=\gamma_{yz}=0$. To solve this problem, reduced order of integration is usually used.[6]

In this study, the reduced order of numerical integration of 2 x 2 Gaussian quadrate was applied to calculate stiffness matrix and equivalent nodal forces. The element has been tested to be free of shear-locking and zero-energy mode within the thickness of the specimens used in the verification.

1. INTRODUCTION

Recently an increasing number of complex reinforced concrete shell structures, such as underground tanks, nuclear waste containers, huge silos, cooling towers, and offshore structures have been built in areas of heavy seismic activitiy. The combination of complexity of three-dimensional geometry and loading conditions, as well as three-dimensional nonlinear behaviors of reinforced concrete make the conventional analysis methods insufficient to predict accurately the behavior of the structures. New and more efficient analytical procedures are needed for this purpose. Nonlinear finite element analysis is becoming one of the most popular procedures used to meet this demand.

This tendency implies that the accuracy of structural analysis will have more dependence on the capability of the analytical tool to predict second order effects which cause nonlinearities. Some important factors that cause nonlinearities in reinforced concrete include tension stiffening, compression softening, and stress-transfer nonlinearities around cracks, which are usually accounted for in the constitutive models of reinforced concrete. Another source of nonlinearity is the geometry of the structure, which is generally considered by the inclusion of second order term of strains in the strain-displacement relationship. Since a standard method to include the effect of geometrical nonlinearity is available, the main factor affecting the level of analytical accuracy remains with the constitutive models installed inside the finite element program.

A lot of effort has been put into the development and application of finite element analyses for reinforced concrete plates and shells.[1),2)] However, a lot of these put emphasis on developing specialized element and efficient solution algorithms with insufficient attention to the implementation of realistic constitutive models that can accurately predict the behavior of concrete shells.[3)] Particularly, realistic constitutive models for reinforced concrete three-dimensional shells under cyclic and reversed cyclic loads have not been adequately addressed. For that reason, finite element programs which are capable of predicting behavior under cyclic and reversed cyclic loads are also limited.

Considering that some of the structures are located in earthquake-prone areas and subjected to dynamic loads, path-dependent three-dimensional nonlinear analysis of shell structures, which is able to predict responses under cyclic and reversed cyclic loads, is indispensable to correctly simulate behaviors of reinforced concrete shells.

At present, a set of constitutive models based on one-dimensional stress fields of cracked concrete and reinforcement are available.[4)] These constitutive models comprise a model of cracked concrete in compression, incorporating compression-softening effects due to transverse cracking; a model of cracked concrete in tension, reflecting tension-stiffening effects due to bond interactions with reinforcement; a model of cracked concrete in shear, reflecting the aggregate interlocking; and a model of reinforcement in reinforced concrete. The models cover loading, unloading and reloading paths. A finite element program incorporating these constitutive models has been used to predict the responses of concrete panels under both in-plane monotonic and cyclic loads successfully.[4)] In fact, this reinforced concrete model is only one code which can deal with two-way cracking accompanying crack opening and closing under reversed cyclic loads.

The purpose of this study is to develop a generic path-dependent three-dimensional reinforced concrete shell element by utilizing the above mentioned two-dimensional constitutive equations and layered formulation as shown in **Fig. 1**. The distinctive characteristic of this element is its capability to simulate behavior of reinforced concrete shell structures under cyclic and reversed cyclic loads. Formulation and verification using test data is presented in this paper. In addition, the need to include the effect of geometrical nonlinearity on thin shells subjected to in-plane and out-of plane loads is also shown.

2. ELEMENT FORMULATION

The choice of element type is important, since it will affect both the application range of the element and the accuracy of the analytical results. Therefore, the nature of the problem, underlying assumptions and the objective of the analysis requires careful consideration.[5)] These considerations should be taken into account maintaining the simplicity of the finite element formulation.

PATH-DEPENDENT NONLINEAR ANALYSIS OF RC SHELLS SUBJECTED TO COMBINED IN-PLANE MEMBRANE AND OUT-OF-PLANE FLEXURAL ACTIONS

(Reprinted from Journal of Materials, Concrete Structures and Pavements, No. 557, V-34, 1997)

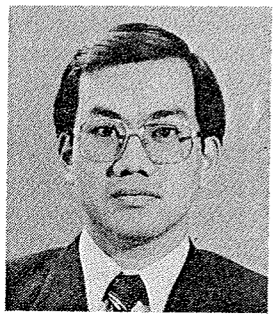

Paulus IRAWAN

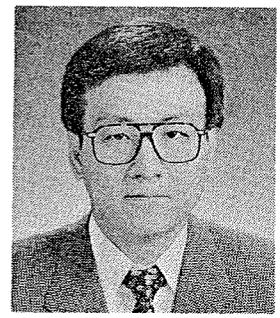

Koichi MAEKAWA

Path-dependent nonlinear finite element analysis is presented for the analysis of reinforced concrete shell structures. Shell element was formulated by utilizing two-dimensional path-dependent constitutive models of reinforced concrete and layered approach. Since the constitutive models cover loading, unloading and reloading paths, the element is capable of predicting behaviors of reinforced concrete shells under cyclic and reversed cyclic loading. The Reissner-Mindlin assumption is adopted to permit the shell to experience shear deformation. Experimental verification under various loading conditions was conducted and the analytical prediction generally gives satisfactory results.

Keywords: reinforced concrete shells, constitutive equations, finite element analysis

P. Irawan is a Lecturer in the School of Civil and Structural Engineering at Nanyang Technological University, Singapore. His research interests relate to mechanical behavior of concrete under triaxial stresses and nonlinear analysis of reinforced concrete members.

K. Maekawa is a Professor in the Department of Civil Engineering at the University of Tokyo. His research interests cover reinforced concrete mechanics, computational approaches to the seismic behavior of reinforced concrete-soil systems, the thermodynamics of cement-concrete composites and the durability design of concrete structures.